NASA Technical Memorandum 81961

NASA-TM-81961 19810014539

TRANSONIC FLUTTER AND GUST-RESPONSE TESTS
AND ANALYSES OF A WIND-TUNNEL MODEL OF A
TORSION-FREE-WING FIGHTER AIRPLANE

Charles L. Ruhlin and Arthur C. Murphy

APRIL 1981

TRANSONIC FLUTTER AND GUST-RESPONSE TESTS AND ANALYSES OF A WIND-TUNNEL MODEL OF A TORSION-FREE-WING FIGHTER AIRPLANE

Charles L. Ruhlin*
NASA Langley Research Center
Hampton, Virginia

and

Arthur C. Murphy[†]
General Dynamics Corporation/Ft. Worth Division
Ft. Worth, Texas

Abstract

An exploratory study of a 1/5.5-size, complete-airplane version of a torsion-free-wing (TFW) fighter aircraft was conducted in the Langley Transonic Dynamics Tunnel. The TFW consisted of a wing/boom/canard assembly on each fuselage side that was interconnected by a common pivot shaft so that the TFW could rotate freely in pitch. The effect of the TFW was evaluated by comparing data obtained with the TFW free and the TFW locked to the fuselage. With the model mounted on cables to simulate an airplane free-flying condition, flutter boundaries were measured at Mach numbers (M) from 0.85 to 1.0, and gust responses at M = 0.65 and 0.90. The critical flutter mode for the TFW-free configuration was found experimentally to occur at M = 0.95 and had the rigid-TFW pitch mode as its apparent aerodynamic driver. However, the minimum flutter dynamic pressure for the TFW-free case was only about 20 percent lower than for the TFW-locked; therefore, the present TFW is considered to be a viable design concept, with respect to flutter. The present TFW was not effective as a gust alleviator. Analyses of the vibration, flutter, and gust-response characteristics were made using a finite-element representation and aerodynamic terms based on lifting-surface theory that included interference effects. Although the analyses predicted the flutter-critical modes, the experimental flutter-speed levels and M trends were predicted poorly. The analytical gust-response data correlated reasonably well with the experimental data.

I. Introduction

A torsion-free-wing (TFW) is defined herein as a wing which is mounted on the fuselage of an aircraft by means of a spanwise oriented pivot shaft and is mechanically unrestrained in rigid-body pitch during flight. Similar types of wings have been referred to as a free-wing or a free-floating wing configuration. An illustration of a TFW on a conceptual fighter-airplane design is the model used in the present study, sketches and photographs of which are presented in figures 1 and 2.

A TFW is designed to have its aerodynamic center located behind its pivot and thus acts as a stable weathervane during flight to maintain an equilibrium pitch attitude. To position a TFW at the desired angle of attack during flight, an aerodynamic trim surface is required. This trim surface can be located forward or aft of the wing and can be attached either directly to the wing or to a structural boom extending from the wing. For example, to place the TFW of the present model at a desired angle of attack during flight, the all-movable canard surface is driven to a predetermined pitch angle on the boom. The resulting lift force on the canard creates a pitching moment about the wing pivot which in turn rotates the wing/boom/canard to an angle of attack where the net pitching moment about the wing pivot is zero. The total lifting force from the wing/boom canard is exerted through the TFW pivot shaft to the airplane fuselage.

One of the potential advantages of a TFW is gust-response alleviation because the TFW is free to pitch and thus relieve the gust. Other potential advantages are shorter takeoff and landing distances, greater maneuverability, and greater design flexibility in the location of the engines, landing gear, and other airplane components. A TFW on a fighter airplane would allow fuselage pointing for better target tracking and ground strafing.

A potential problem of a TFW airplane is flutter. To alleviate a gust effectively, the TFW must react by pitching to a new angle quickly enough to relieve the gust, hence, it must have a reasonably high pitch frequency. However, if the free-wing pitch frequency is near the wing structural bending frequency, the wing could become susceptible to a bending-pitch type of flutter, and the flutter speed may be unacceptably low. Conversely, if the free-wing pitch frequency becomes too low, it may couple unfavorably with the rigid-body modes.

The adequacy of current analytical methods to predict the flutter and gust-response characteristics of a TFW vehicle at transonic speeds is uncertain because of the difficulty in accounting for the freely pivoting TFW motion. Little, if any, experimental data were available with which to assess the accuracy of the analytical methods when applied to a TFW airplane in the transonic range.

To provide some experimental data, therefore, an exploratory investigation was conducted in the Langley Transonic Dynamics Tunnel (TDT) to determine the transonic flutter and gust-response

---

*Aero-Space Technologist, Configuration Aero-elasticity Branch, Loads and Aeroelasticity Division.

[†]Engineering Specialist, Structural Dynamics Group, Structures Section, Structures and Design Department.

N81- 23072

characteristics of a TFW airplane model. The model was a 1/5.5-size version of a conceptual supersonic fighter airplane that had been studied analytically at the General Dynamics/Ft. Worth Division (GD/FW). The effect of the TFW was evaluated by obtaining data both with the TFW free and with the TFW locked to the fuselage. All significant flutter and gust-response data were obtained with the model supported on a cable-mount system that simulated a near free-flight condition. Initial, limited tests were made with the model mounted on a sting to examine the stability of the freely pivoting TFW at transonic speeds.

Vibration, flutter, and gust-response analyses were made for correlation with the experimental data. The analyses employed a NASTRAN* finite-element structural representation of the model and aerodynamic terms that were based on lifting-surface theory and included aerodynamic interference effects. Some aspects of the analytical approach are noteworthy. First, because there was a slight asymmetry in the model wing panel masses, all calculations employed a complete wing-tip to wing-tip analytical model. Second, the flutter and gust-response analyses were made using both measured and calculated vibration modes and frequencies to determine the sensitivity of the flutter and gust-response characteristics to differences in these modal data. Finally, to determine the effect of the free-pivoting TFW on the gust response in a realistic aircraft environment, both the experimental and analytical gust-response transfer functions were converted to equivalent full-scale airplane quantities, and the response to a von Karman atmospheric gust spectrum was then determined for each case.

The significant results and trends from these experimental and analytical studies are presented in this paper. A more detailed report on these studies is available in reference 1, which includes the model physical properties and other data in sufficient detail to permit independent analyses.

II. Model

General

On the present 1/5.5-size wind-tunnel model only the planforms of the wing/boom/canard surfaces and the wing airfoil geometry were closely scaled from the conceptual airplane. In general, the model was designed and constructed to be as simple, strong, and inexpensive as possible. The wing surface, however, was designed to have a representative spanwise distribution of mass and stiffness and to flutter in the wing-locked configuration within the operating dynamic pressure range of the Langley TDT. The other model components were relatively stiff compared to the wing surface.

The free-pivoting TFW consisted of a wing/boom/canard assembly (figures 1 and 2) on each airplane side that was interconnected by a common pivot shaft that passed through and was supported by bearings in the fuselage. Thus, both sides

---

*NASTRAN: Registered trademark of the National Aeronautics and Space Administration.

of the wing/boom/canard assembly pivoted freely and symmetrically in pitch. To obtain the TFW-locked condition, each boom was bolted to a side of the fuselage about 0.30 m (12 in.) forward of the wing pivot. During the tests, the pitch attitude of the TFW was set by remotely controlling the all-movable canards. This was done by a pilot in the tunnel control room who also independently controlled the roll and pitch attitudes of the fuselage by differentially or symmetrically pitching the all-movable horizontal tails.

Two modifications to the basic model configurations were made during the tunnel tests: (1) a reduction in the original canard area by about 40 percent and (2) the addition of the ventral fins. All data presented herein are for the final, modified configuration.

The mass properties of the model and its components are summarized in table I. After the tunnel tests, the left wing surface was found to be 0.227 kg (0.5 lbm) heavier than the right wing (see table I). This weight mismatch, which amounted to about 6 percent of the wing surface weight, resulted apparently from an unequal application of the surface finish to the wing.

Construction

Each wing structure consisted of a solid aluminum-alloy plate that was tapered spanwise in thickness to produce a representative distribution of mass and stiffness. End-grain balsa wood blocks were bonded to this plate and contoured to form a 4-percent-thick, symmetric airfoil shape. A soft epoxy finish was applied over the balsa surface to provide a smooth, moisture-proof surface.

Each boom was mainly rectangular in cross-section and consisted of thin aluminum plates bolted together to form a hollow box. The outboard wall of the boom had an integrally machined shelf to which the wing was bolted. The inboard wall of the boom was machined integral with a hollow pivot shaft. Within the fuselage, enclosed in the interconnected TFW pivot shaft, were the electric motors which controlled the canard pitch attitude. The remaining drive mechanisms from the motors to the canards were housed inside the boom.

Each canard surface was a thin aluminum plate with rounded leading and trailing edges. The canard plate root was attached to a pivot shaft that was supported by bearings in the boom so that the canard was all-movable in pitch.

The model fuselage simulated that of an airplane having twin jet engines located in the rear of the fuselage and having a large, ramp-like engine inlet on each side of the fuselage. The main, center portion of the fuselage was rectangular in cross-section and was constructed as a semi-monocoque body by forming an aluminum sheet into a hollow shell structure to which was attached longitudinal stiffeners and several transverse bulkheads. The remaining fuselage sections were made from aluminum tubing and balsa wood fairings.

The vertical and horizontal tail surfaces were stiff, lightweight surfaces borrowed from another flutter model. The all-movable horizontal

tails were mounted on spindles and controlled symmetrically or differentially in pitch by drive systems housed in the fuselage. The ventral fins were two thin aluminum plates that were cantilever-mounted from the lower outboard corners of the fuselage.

Instrumentation

The model was equipped with accelerometers to measure vertical motions at five different stations along the fuselage centerline: these included the pilot station, model center of gravity, and the midpoint between them. Strain gages were mounted near each wing root to measure the bending and torsion moments, near each canard root to measure bending moments, and near each horizontal tail root to measure bending moments. The TFW pitch angle relative to the fuselage was measured by means of a potentiometer that was attached to the TFW pivot shaft. The fuselage pitch angle was measured by a servo-accelerometer mounted to the fuselage. The canard pitch angles were monitored visually.

III. Finite-Element Model

The model structure was represented by a finite-element structural model by using the MSC/NASTRAN structural analysis computer program.[1] The general arrangement of the finite-element model is shown in figure 3. The wings and canards were modeled primarily with plate elements. For the wings, the contributions to stiffness and mass of both the aluminum plate and balsa wood covering were accounted for in the structural model. Differences between the right and left wings were accounted for also. The fuselage and booms were modeled with beam elements. The wing-boom attachment was represented by a combination of spring and bar elements. The TFW pivot shaft was represented by a beam element. The pivot shaft was free to pitch relative to the fuselage. The TFW-locked condition was simulated by rigidly attaching each boom to the fuselage at the appropriate chordwise station. The representation of the empennage and ventral fins was rather coarse and primarily accounted for only mass and inertia effects of these components. A detailed description of the finite-element model is given in reference 1.

IV. Vibration Characteristics

General

The vibration characteristics of the model in the TFW-free and TFW-locked configurations were determined both experimentally and analytically. The experimental modes were measured in a ground vibration test (GVT) after the wind-tunnel test. The analytical modes were computed using NASTRAN.

Presented in table II are the measured and calculated frequencies and associated measured damping ratios of the natural vibration modes used in the flutter and gust-response analyses. In the table, each model surface that participated significantly in a vibration mode is identified, and the surface (or surfaces) whose motion predominated is indicated by an underline. Most of the GVT modes exhibited either symmetric or antisymmetric motion although some asymmetry was

present in all of these modes. Many calculated modes involved motion primarily on one vehicle side only and are listed as asymmetric modes in the table. The fact that only a single mode was sometimes measured where two modes were calculated, one associated with a left-wing resonance and one with a right-wing resonance, is believed to be caused by the damping and friction physically present in the model which were not represented in the NASTRAN analyses. Figure 4 shows the mode shapes of the fundamental symmetric wing bending and torsion modes. More detailed vibration mode data are presented in reference 1.

GVT Measurements

In the ground vibration test, the model was supported by four, overhead soft springs attached to the fuselage. A very soft spring (rubber band) was used to support the wings in a level pitch attitude relative to the fuselage. Because all rigid-body frequencies of the model on this mount were below 1 Hz, the measured modes are believed to represent the free-free condition. The measured rigid-body frequencies presented in table II are those for the model mounted on the wind-tunnel cable-mount system. These cable-mount rigid-body frequencies are considered to be sufficiently low so as to have little or no effect on the flexible modes.

Up to four lightweight electro-magnetic shakers were used to excite the model. The modal amplitudes were measured by means of a roving-and-reference accelerometer method. The mass of each accelerometer and associated equipment was less than one gram.

Vibration Analysis

The free-free modes and frequencies of the model, including elastic and rigid-body modes, were calculated by using the complete wing-tip to wing-tip NASTRAN finite-element model described previously. Modal data were calculated for both the TFW-free and TFW-locked cases. Rigid-body fore-and-aft translation was restrained in the analysis so only five rigid-body modes were determined. For the TFW-free case, a rigid-TFW pitch mode was calculated in addition to the complete model rigid-body modes.

To improve the experimental-analytical correlation in the wing primary modes, it was necessary to increase the elastic moduli of the wing aluminum plate structure by about 26 percent from the nominal values. The final moduli used were $E = 9.14 \times 10^7$ kN/m^2 (13.25×10^6 lb/in.^{2}) and $G = 3.47 \times 10^7$ kN/m^2 (5.04×10^6 lb/in.^{2}). This increase was required to account for the stiffening effect of the surface epoxy finish which was not modeled directly in the NASTRAN representation. All data presented herein were obtained by using the adjusted module.

Experiment-Analysis Correlation

The experimental vibration modes were measured as carefully as conditions permitted but were found to be somewhat non-orthogonal because the generalized mass matrices, determined by using the measured mode shapes and computed mass distributions, had off-diagonal terms of

appreciable magnitude. Because the analysis predicts only the normal orthogonal vibration modes, some differences in correlating the modal data could be expected.

The correlation of the experimental and analytical vibration modes is quite good for the lower frequency flexible modes. As the frequency increases, however, the disagreement between the two becomes greater. The analytical modes were considered to be acceptable because the flutter cases encountered in the wind-tunnel tests apparently involved the lower frequency modes and the gust-response tests of the model covered a frequency range which extended from near zero to a frequency slightly higher than the first flexible mode. A further consideration regarding the poor agreement in the higher frequency modes is that most of the GVT modes above 40 Hz involved significant motion of the fuselage and tail surfaces which were not represented in the finite-element model to the same detail as the TFW surfaces.

To examine the effects of these differences between these data on the flutter and gust-response characteristics, analyses were conducted using both the GVT and NASTRAN vibration modes.

V. Test Apparatus and Procedures

Wind Tunnel

The wind-tunnel tests were conducted in Freon-12* in the Langley Transonic Dynamics Tunnel (TDT). This tunnel has a 4.88-m (16-ft)-square, slotted test section with cropped corners and is capable of operating at Mach numbers up to 1.2 in air or Freon-12 over a wide range of test-medium densities. Mach number and dynamic pressure can be varied simultaneously or independently. The tunnel is equipped with four, quick-opening bypass valves which, when actuated, can reduce rapidly the Mach number and dynamic pressure in the test section.

Gust Generating System

The TDT is equipped with a gust-generating system that produces a gust field of sinusoidal, oscillating, vertical perturbations in the stream flow at the test section.[3] The gusts are generated by oscillating in pitch two pairs of vanes located upstream of the test section as shown in figure 5. The amplitude of the gust field is controlled by varying the amplitude of the vane pitch oscillations. Gust frequencies up to 20 Hz can be generated.

A symmetric gust field was generated for the present tests. This symmetric gust field has been measured and found to be sufficiently uniform over a sizeable region near the center of the test section to permit uniform gust analyses.[3] The wing span of the TFW model was well within this region. The variations of the gust zero-to-peak angular amplitudes (tan ε_g = vertical gust velocity/freestream velocity) with gust frequency

are presented in figure 6 for the two Mach numbers at which data were measured. It can be seen that the gust amplitude decreases with increasing frequency so that, at a frequency of 15 Hz, the model experiences a gust excitation level about 1/3 to 1/7, depending on the Mach number, of that at 0.5 Hz.

Model Mount System

For the initial tests of the model with the TFW free, the model was mounted to a sting as shown in figure 2(a). The sting was attached rigidly to the lower surface of the model fuselage near the wing pivot. Thus, the model was restrained in a safe manner in the event that a TFW instability was encountered.

For all other tests, the model was mounted on a cable system that provided a near free-flying condition (see fig. 2(b)). On this system, the model fuselage is supported on the tunnel center-line by two cables that lay in the vertical plane of the tunnel. Viewed from the model side, the cable arrangement resembled an "X" shape, with one cable extending forward, one cable extending rearward, and both joined at the model to close the X shape at the center. The ends of each cable were pinned to the model fuselage, forming a closed loop that ran from the model through the ceiling, around the test section, and back through the floor to the model. Low-friction pulleys were used to guide the cables in this circuit. At the model, all the cables were oriented at about 45⁰ to the horizontal plane. The rear cable loop included a spring that could be remotely controlled to adjust the tension in this loop. In addition, four safety cables (snubbing system) were attached to each corner of the fuselage shell at a body station near the model center of gravity. These cables passed transversely across the tunnel from the model through the sidewall slots and then to a remotely-controlled damper-piston actuator system. When the snubbing system was actuated, the safety cables would restrain the model in its centerline position.

Tunnel Test Procedure

The wind tunnel was operated either by holding a constant total pressure and increasing Mach number (M) or by holding M constant and increasing dynamic pressure (q). With the model on the cable-mount system, the Mach numbers were limited to values less than 1.0 to avoid a model rigid-body lateral instability. When flutter was encountered, the four bypass valves were actuated to reduce the M and q in the test section, and the flutter subsided very quickly. In the gust-response tests, the tunnel M and q were held constant while the gusts were varied linearly and slowly in frequency from about 0.1 to 18 Hz.

During the tests, the dynamic responses and static loads of various model components were visually monitored on direct readout, oscillograph recorders. Selected model dynamic response data were recorded on analog magnetic tape. A real time analyzer was used to monitor the frequency spectra of the dynamic response of selected model components.

---

*Freon: Registered trademark of E. I. du Pont de Nemours Co., Inc.

4

During the tests of the model on the cable-mount system, the model was flown in a reasonably level condition in the center of the test section by the pilot. For the TFW-locked configuration, model control in roll and pitch was provided by remote control of the all-movable horizontal tails. In the TFW-free tests, the wing pitch angle was controlled by the canards, and the fuselage attitude was controlled by the horizontal tails. The model controls provided adequate and smooth responses, and the pilot could keep the model trimmed without undue difficulty. Typically, the TFW and canard deflection angles were relatively small, e.g., the pitch angle of the TFW relative to the fuselage was kept within $\pm 3°$, and the canard angles relative to the boom were within $\pm 4°$.

VI. Analytical Procedures

General

The aerodynamic forces used in the analyses were calculated by using a GD/FW-developed method which can treat multiple-surface configurations with aerodynamic interference at subsonic, supersonic, or mixed-flow conditions.[4] Only subsonic flow conditions were used in this study.

Steady-state aerodynamic forces were calculated to determine the pitch (weathervane) stability of the original and final wing/boom/canard configurations. Flutter and gust-response analyses were conducted for the TFW-free and TFW-locked configurations using both GVT and NASTRAN modal data. These analyses used complete (tip-to-tip) span modal data in calculating the generalized masses and aerodynamic forces. As a check, the complete-span aerodynamic terms for a TFW-free configuration were compared to those calculated by a conventional half-span analysis modified to include the modal asymmetry, and the agreement was very good.

The aerodynamic normal-wash collocation points used in the analyses were distributed over all lifting surfaces of the tip-to-tip model, although a much smaller number of points were assigned to the fuselage and tail surfaces than to the TFW surfaces. The fuselage, wings, booms, canards, and horizontal tails were all treated as co-planar, horizontal surfaces. The number of normal-wash points assigned to each surface in the spanwise and chordwise direction, respectively, are listed in the parentheses as follows: each wing (5 x 5), each canard (2 x 2), each boom (1 x 5), each horizontal tail (4 x 2), and the total-fuselage (2 x 4). Thus, the wing surface was represented by a grid of 25 panels, the canard by 4, etc. The surfaces lying in a vertical plane were the vertical tail, the ventral fins (the two were lumped together as a single surface), and the fuselage sides. These were all assumed to lie on the centerline of the model. The number of normal-wash points assigned to these surfaces were: vertical tail (1), ventral fins (1), and fuselage sides (4).

Flutter Analyses

Flutter analyses using both the GVT and NASTRAN vibration modes were made at M = 0.65, 0.86, 0.90, 0.95 and 0.975. The analyses

employed all the rigid-body and flexible surface modes listed in table II. At each of these M, a flutter dynamic pressure was calculated for a velocity that exactly matched that in the TDT at that M. This technique was used because, in normal operation of the TDT, the flow velocity remains essentially the same for a given M regardless of the dynamic pressure level. Typically, V-g data were generated at one M for each of six density values, and the resulting flutter data cross-plotted to obtain the matched point. Flutter frequencies were also calculated in this procedure. A nominal damping value g of 0.02 was used for the NASTRAN-calculated flexible modes, and the measured g values were used for all GVT modes (rigid-body and flexible). The calculated rigid-body modes (f = 0 Hz) were replaced by the corresponding measured rigid-body frequencies and damping ratios (table II). This was done because the rigid-body frequencies of the model mounted on the cable system, although small in value, were not equal to zero. The rigid-TFW pitch mode was assigned a frequency of 0.0033 Hz and damping value of g = 0.10 for all TFW-free analyses. Calculated mode shapes were used for all rigid-body modes.

Gust Response Analyses

Gust-response analyses were conducted on an equivalent full-scale airplane at M = 0.65 and 0.90 and at conditions scaled from the wind-tunnel test conditions. Response to gust was calculated for three fuselage accelerations and for wing and canard bending moments. The analytical procedure was to calculate the response of the generalized coordinates due to a unit sinusoidal gust and then in turn calculate the transfer function for each response item. This was done for about 200 discrete frequencies extending over a range from zero to 7 Hz (full scale). The response power-spectral-density (PSD) was then calculated by multiplying the input von Karman atmospheric power spectrum by the square of the absolute value of the transfer function. The rms ($\overline{A}$) values were obtained by taking the square root of the integrated area under the PSD curve. The characteristic frequency (N_0) was computed by taking the square root of the integral of the PSD x (frequency)^2 over the PSD spectrum and dividing by the $\overline{A}$ value. To reduce computer time, the analysis was limited to the modes that were considered to be most significant to a particular response. The modes are as follows:

	Fuselage Accelerations	Bending Moments
TFW-Free Case	First 4 modes	First 7 modes
TFW-Locked Case	First 6 modes	First 6 modes

These modes included the rigid-body vertical translation, pitch, and rigid-TFW pitch modes (for the TFW-free case only), and the remainder were flexible modes. For all analyses, each rigid-body mode was assigned the frequency and damping values used in the flutter analysis described previously.

VII. Stability Results and Discussion

Experimental Results

The initial test of the TFW conducted at low

speeds with the model sting-mounted showed that the wing/boom/canard was unstable in pitch. The instability manifested itself in an unusual way. The TFW would initially assume a fairly large angle of attack of about $10°$ to $12°$, either positive or negative. The canard pitch angle would then be changed and the TFW would move toward the neutral position. As the TFW approached a $3°$ or $4°$ angle of attack, it would swing completely through the neutral position to a $10°$ to $12°$ angle of attack in the opposite direction. This action was confirmed by several repetitions and at different tunnel conditions.

Tufts were added to the model in an attempt to understand this behavior. From observations of the tufts, it appeared that at small angles of attack, the flow on the canard was attached and thus the canard was completely effective aerodynamically. When an angle of attack of $+10°$ to $12°$ was reached, however, the canard would stall or partially stall, lose a portion of the lift and thus shift the overall center of pressure aft and the system would become aerodynamically stable. This instability was solved by reducing the canard size to one having 60 percent of the original canard area.

Analytical Correlation

The steady state aerodynamic lift and center of pressure (c.p.) were calculated for the TFW with the original large canard and the final small canard. This was done as a two-fold check: (1) to verify that the instability observed experimentally was due to the aerodynamic loading as surmised from the tuft study, and (2) to verify that the analytical method was sufficiently accurate to predict this instability and the fix. As a sub-case of the flutter analyses for $M = 0.65$, the aerodynamic loads were calculated for steady flow (reduced frequency = 0) and for the TFW at a unit angle of attack. These results showed that the calculated center of pressure of the TFW with the original canard installed was about 1.25 cm (0.5 in.) ahead of the wing pivot axes and with the 60-percent area canard installed was 0.89 cm (0.35 in.) behind the wing pivot axes. Thus the TFW was predicted to be aerodynamically unstable in pitch with the original canard and stable with the final, smaller canard. It also appeared that the aerodynamic program was predicting the loads on the TFW and accounted for the interference effects between these surfaces. It is of interest to note that of the total lift force predicted for the TFW with the small canard, 77 percent came from the wing, 11 percent came from the boom, and 12 percent from the canard. Of the total TFW area, each of these surfaces had 79 percent, 14 percent, and 7 percent, respectively.

Other analyses were conducted in an effort to predict the stability at higher angles of attack obtained with the original canard configuration. Analyses were made with the canard displaced vertically out of the wing/boom plane (1) by 5 cm (2 in.), (2) by 12.5 cm (5 in.), and (3) with all three surfaces on the same plane but with no interference effects. The 5 cm canard displacement was approximately equivalent to its location when the TFW was

rotated to about a $5°$ pitch angle. All of these analyses indicated that the TFW would still be statically unstable although the c.p. was moved aft somewhat. Apparently, the original canard had to reach a stalled condition for the configuration to be stable.

VIII. Flutter Results

Experimental Results

With the model mounted on the cable system, the flutter characteristics for both the TFW-free and TFW-locked configurations were determined at Mach numbers from about 0.85 to 1.0. Tunnel schedule limitations did not permit sufficient time to define the flutter boundaries in more detail. The experimental flutter boundaries are plotted in figure 7 in terms of the dynamic pressure required for flutter against Mach number. (The flow velocity V in m/sec at these points can be computed from the relationship $V = 153 \times M$.) All of the experimental flutter modes were basically symmetric. The flutter frequency at each flutter point is included in figure 7.

Except for the low-frequency flutter of the TFW-free configuration, it was difficult to distinguish the exact onset of the wing flutter from the lowly damped, sinusoidal motions preceding flutter. In this low-damped region, the response of the left wing was significantly greater than the right, and there was a beating between the motions of the two wings. The amplitude and duration of these motions gradually increased as the flutter point was approached until, at the designated flutter point, the motions of each wing were of sizeable amplitude, sinusoidal, and nearly sustained.

The two flutter points obtained with the TFW-locked formed a conventional looking, transonic-flutter boundary shape (See fig. 7). The flutter mode appeared to involve a classical coupling of the fundamental bending and torsion modes of the wing surface with very little motion of the other surfaces.

With the TFW-free, at $M = 0.9$, the wing surface fluttered in a mode similar to that for the TFW-locked configuration but at a somewhat higher q. At M near 0.95, the TFW-free configuration fluttered in a benign, low-frequency mode that appeared to involve a coupling of the rigid-TFW pitch and wing-surface first-bending mode. The flutter boundary defined for this mode showed (fig. 7) a very steep drop in dynamic pressure at a nearly constant Mach number to a value about 20 percent less than that for the TFW-locked case. Because of a possibility that the flutter may be influenced by the relative pitch attitudes of the TFW and fuselage, each low-frequency flutter point was repeated with a different combination of pitch angles for these components with essentially the same result.

Thus, this lower frequency mode became the flutter-critical mode for a TFW at transonic speeds. This mode is expected to be a serious concern in the flutter design of a TFW airplane because the rigid-TFW pitch mode is apparently the aerodynamic driver in this flutter instability, and its frequency is very sensitive to

changes in the c.p. location of the TFW. However, because the TFW-locked configuration was much like a conventional, fixed wing which would necessarily have to be flutter free, the 20-percent reduction in flutter q obtained with the TFW free was not considered large enough to make a TFW unacceptable from a flutter standpoint as a viable design concept.

Why, at M = 0.9, the free configuration fluttered in a similar flutter mode as the TFW-locked configuration but at a higher q is not known. Comparison of the frequencies and mode shapes of the primary bending and torsional modes shows only minor differences between the two configurations (See fig. 7 and table II). It is hypothesized that some of the higher frequency modes may influence the flutter differently for the TFW-free case than the TFW-locked case or that the TFW-free flutter may be affected by the rigid-TFW pitch mode.

Analytical Correlation

Flutter analyses were made for the two test configurations at M = 0.65, 0.86, 0.90, 0.95, and 0.975. The results are presented in figure 8 as flutter boundaries expressed in terms of the flutter speed V_F in knots equivalent air speed (KEAS) against Mach number. (This V_F was based on a selected model density value $\rho = 2.741$ kg/m^3 (.0053018 slug/ft^3) that would give roughly comparable full scale KEAS values if the model flutter test results were converted to full scale quantities.) The results of the analyses using the GVT modal data and the NASTRAN modal data are plotted separately, and the experimental flutter points are included on each plot for comparison.

For the TFW-free case (fig. 8(a), both the low- and high-frequency flutter roots were predicted by use of either the GVT or NASTRAN modes in the analyses. The GVT-mode analyses predicted the low-frequency root to be critical at all Mach numbers, whereas the NASTRAN-mode analyses predicted the two different roots to cross each other at about M = 0.85. Below this M, the high-frequency root is critical, and above this M, the low-frequency root is critical. It appears that the NASTRAN-mode analyses predicted the experimental trends somewhat better than did the GVT-mode analyses.

For the TFW-locked case (fig. 8(b)), both analyses predicted two instabilities. One varied in frequency over the Mach range from 17 to 22 Hz, while the other varied from 19 to 24 Hz. The 17 - 22 Hz root is believed to best correspond to the experimental data.

Overall, the analysis-experiment correlation in the flutter speeds and Mach number trends is rather poor. Nevertheless, the analyses did predict the experimental flutter-critical modes. In attempts to improve the correlation, several changes to the analytical procedure were made including changing the number of wing normal-wash collocation points, excluding fuselage aerodynamics, eliminating aerodynamic interference effects of the canard on the wing, assigning zero values to the rigid-body frequencies at zero airspeed, and for the GVT modes, replotting and

smoothing the modal deflections. None of these produced any substantial changes in the analytical results.

It is believed that the poor correlation stems primarily from the effects of the wing mass asymmetry on both the test and analytical results. In the wind-tunnel tests, the high-frequency flutter for both configurations was preceded by a low-damping region, characterized by much larger amplitudes on the left wing than on the right, that made the onset of flutter difficult to identify. From an analysis standpoint, the tip-to-tip aerodynamic modelling may not be entirely adequate because of the computer program limitation on the number of collocation points. In any event, it is recommended that, in any future TFW-airplane design, the flutter analysis should be validated by experiments as early as possible.

IX. GUST RESPONSE RESULTS

Experimental Results

The model response to the symmetric gust-field generated in the TDT was measured at the following two test conditions:

M	q	V
0.65	2.873 kPa (60 lb/ft^2)	99.5 m/sec (326 ft/sec)
0.90	4.788 kPa (100 lb/ft^2)	137.8 m/sec (452 ft/sec)

At each condition, the gusts were varied slowly and continually from about 0.1 to 18 Hz at a linear rate of about 4 Hz/min. Data were processed for the following five model parameters: vertical accelerations at (1) the pilot station, (2) model c.g., (3) a fuselage station midway between the preceding stations, and root bending moments on the (4) left wing ana (5) left canard surface.

Measured gust-response spectra are presented in Figure 9 for the pilot station accelerations and the wing bending moments. These results are typical of the response data at the other stations. These spectra represent the maximum response amplitude that was obtained at a particular frequency during a gust frequency sweep. It can be seen (Fig. 9) that freeing the TFW reduced the response slightly in the two rigid-body modes at f < 2 Hz but increased the response from f = 3 to 15 Hz. The rigid-TFW pitch mode was apparently near 3 Hz, and the wing first-bending mode near 13 Hz. Overall, freeing the TFW seemed to have increased rather than decreased the model gust response.

To determine the effect of the TFW in a realistic airplane flight environment, the model responses to atmospheric gust turbulence were scaled up to full-scale airplane quantities. Scaling ratios of the present model to the conceptual TFW airplane were derived and are presented in Table III. The atmospheric gust turbulence was represented by the von Karman gust power spectral density (PSD) plotted in Figure 10 in full-scale units for each of the two test Mach numbers. The von Karman PSD function ϕ_i is:

$$\Phi_i = 2\pi \; \sigma^2 \; \frac{L}{\pi V} \left\{ \frac{1 + \frac{8}{3} \left(1.339 \; \frac{L2\pi f}{V} \right)^2}{\left[1 + \left(1.339 \; \frac{L2\pi f}{V} \right)^2 \right]^{11/6}} \right\}$$

where
- σ = 0.3048 m/sec (1 ft/sec)
- L = 152.4 m (500 ft)
- V = 207 m/sec (679 ft/sec) at M = 0.65
- V = 286 m/sec (940 ft/sec) at M = 0.90
- f = gust frequency, Hz

The procedure followed was (1) to calculate a transfer function for each parameter from its response to the tunnel gusts, (2) to convert each transfer function to full-scale airplane units, and (3) use each transfer function to calculate the response PSD to the von Karman gust spectrum. The resulting response PSD plots are presented in Figure 11(a) for the pilot-station acceleration. Compiled in Table IV for the fuselage accelerations are the integrated, root-mean-square (rms) values ($\bar{A}$) and characteristic frequency values (N_o). These results are fairly typical of the data for the other reduced parameters.

The PSD plots of the experimental data show (Fig. 11(a)) the effect of the concentration of the atmospheric gust power in the low-frequency range (f < 1 Hz). Above 1 Hz, the response is increasingly attenuated by the decrease in the atmospheric turbulence power so that the gust-response characteristics at the higher frequencies become much less significant. A comparison of the $\bar{A}$ values (Table IV) indicates that, in general, freeing the TFW increased the gust response slightly rather than reduced it. It is surmised that this may be caused by the present TFW configuration having too low a rigid-TFW pitch frequency (i.e., the TFW center of pressure was too close to the TFW pivot) to reduce the gust response appreciably.

Analytical Correlation

The gust-response data calculated using the GVT and NASTRAN modal data are included in Figure 11 and in Table IV for comparison with the experimental data. Overall, the calculated gust-response data are considered to be in reasonable agreement with the experimental results. The calculated PSD plots indicate the same basic pattern as the experiments although the frequencies at which the peak responses occur do not correspond very well. The GVT-mode analyses nearly always indicate a reduction in the response $\bar{A}$ levels when the TFW was freed, whereas the NASTRAN-mode analyses indicate either a reduction or increase, depending on the response parameter. While the $\bar{A}$ levels for either analysis never consistently agree with the experimental values, neither are they particularly bad.

The analytical-experimental correlation might be improved on a different TFW configuration for the following reasons. First, the gust responses which are most affected by the TFW are seen to be primarily in the low-frequency, rigid-body modes which could be affected by possible non-linearities in the damping and spring-rates of the cable-mount system on which the model was suspended. Secondly, in the present TFW-free configuration, the TFW c.p. is very close to the wing pivot, and small shifts in this c.p. during the model oscillation could affect appreciably the response amplitude. Similarly, in the analysis for the TFW-free case, a small error in computing the TFW c.p. could possibly affect the overall calculated responses.

X. Conclusions and Recommendations

Analytical and exploratory wind-tunnel studies of the transonic flutter and gust-response characteristics of a complete TFW fighter-airplane model have been made. Flutter boundaries were measured at M = 0.85 to 1.0, and gust responses at M = 0.65 and 0.90. The effect of the TFW was evaluated by comparing data obtained with the TFW free-to-pitch and the TFW locked to the fuselage. The results of these studies have indicated the following conclusions:

1. The present TFW configuration is considered to be a viable design concept from a flutter standpoint because the TFW-free configuration fluttered at a dynamic pressure only about 20 percent lower than did the configuration with the TFW locked to the fuselage.

2. For the TFW-free configuration, the flutter critical mode was encountered in a narrow Mach number region near 0.95 and consisted of a coupled TFW-pitch and primary wing-bending motion. This mode could be a serious concern in the flutter design of a TFW airplane because it may be very sensitive to changes in the center-of-pressure location of a TFW.

3. Although the flutter analyses predicted the experimental flutter-critical modes, the experimental flutter dynamic pressure levels and Mach number trends were predicted rather poorly.

4. The present TFW configuration was not effective as a gust alleviation design probably because the TFW center of pressure was too close to the pivot axis.

5. The gust-response characteristics predicted by analyses correlated reasonably well with the experimental results.

6. The use in the analyses of NASTRAN-calculated modal data rather than measured modal data affected primarily the predicted flutter speeds. Because of the overall poor analysis-experiment correlation, it is inconclusive as to which set of modal data gives the better design information. Flutter and gust-response analyses of future TFW designs should be verified experimentally as early as possible.

It is recommended that:

1. Additional experimental studies should be made to establish the viability of the TFW concept, both from a flutter and gust-response point of view. In particular, the effect of moving the TFW center of pressure should be examined.

2. In any future wind-tunnel testing of a TFW, procedures similar to the present test methods should be used but with the following improvements:

(a) A criteria should be developed to distinguish the onset of flutter from the low-damped response of the model, particularly of a model having a significant degree of asymmetry.

(b) The damping and any nonlinear characteristics of the rigid-body modes of the model on the mount system should be closely examined.

(c) Gust-response measurements should include variations in gust amplitude to prove linear response characteristics.

XI. References

[1]Murphy, Arthur C., "An Experimental and Analytical Study on the Flutter and Gust Response Characteristics of a Torsion-Free Wing Airplane Model," NASA CR-159283, 1981.

[2]MSC/NASTRAN Users Manual. MacNeal-Schwendler Corporation Report MSR-39, Rev. 1978.

[3]Redd, L. Tracy, Hanson, Perry W., and Wynne, Eleanor C., "Evaluation of a Wind-Tunnel Gust Response Technique Including Correlations with Analytical and Flight Test Results," NASA TP-1501, 1979.

[4]Cunningham, Atlee M., Jr., "A Steady and Oscillatory Kernel Function Method for Interfering Surfaces in Subsonic, Transonic, and Supersonic Flow," NASA CR-144895, 1976.

TABLE I. MODEL MASS PROPERTIES.

Component		Mass (kg)	c.g. FS(m)
TFW	Wing (Left)	4.209	-
	Wing (Right)	3.983	-
	Boom (Each)	3.402	-
	Canard (Each)	.268	1.372
	Pivot shaft (Each)	.050	1.891
TFW (Right)		7.703	1.883
TFW (Left)		7.929	1.883
Fuselage		65.727	1.592
Horizontal Tails		1.098	2.891
Vertical Tail		.948	2.891
Ventral Fins		.726	2.926
Total model		84.131	1.692

Inertia about c.g. -
Pitch: TFW (Left)   = 0.8422 kg-m^2
       TFW (Right) = 0.8311 kg-m^2
       Total model = 62.712 kg-m^2
Yaw: Total model = 66.427 kg-m^2

TABLE II. MEASURED AND CALCULATED VIBRATION-MODE CHARACTERISTICS

Mode Code: Example W1B = Wing 1st bending.

W: Wing   S: Horizontal Stabilizer   B: Bending
F: Fuselage   V: Vertical Stabilizer   T: Torsion
C: Canard

| Mode | Measured (GVT) | | | | Calculated (NASTRAN) | | | |
| | Symmetric | | Antisymmetric | | Symmetric | Antisym-metric | Asymmetric | |
	f (Hz)	g	f (Hz)	g	f(Hz)	f(Hz)	Left f(Hz)	Right f(Hz)
Rigid-body modes for both model configurations								
Vertical translation	0.92	0.4	-	-	0	-	-	-
Pitch	0.76	.04	-	-	0	-	-	-
Side translation	-	-	1.05	-	-	0	-	-
Roll	-	-	1.95	-	-	0	-	-
Yaw	-	-	0.4	-	-	0	-	-
TFW-free configuration								
Rigid-TFW pitch	0	-	-	-	-	-	-	-
W1B	13.7	.063	17.5	.081	14.26	16.91	-	-
W1T	36.3	.088	36.7	.063	-	-	33.20	34.75
WB, SB, CB, F1B	44.3	.02	-	-	-	-	-	-
W2B	-	-	-	-	-	-	48.23	50.06
W2B, SB, CB	54.3	-	-	-	-	-	-	-
WB, SB, CB, V1B	-	-	58.0	.036	-	-	-	-
C1B	68.3	.037	68.1	.036	-	-	-	-
W2T, CB	-	-	-	-	-	-	67.22	70.15
WB, C1B	-	-	-	-	-	-	75.25	73.63
C1T	-	-	-	-	-	-	78.84	-
W2T - right wing	83.5	.063	83.3	.068	-	-	-	86.82
W2T - left wing	88.1	.088	88.0	.082	-	-	84.11	-
W2T	-	-	-	-	89.13	-	-	-
TFW-locked configuration								
W1B	12.6	.063	15.2	.063	12.67	16.93	-	-
W1T - left wing	36.0	.049	35.8	.063	-	-	32.96	-
W1T - right wing	36.4	.073	36.3	.063	-	-	-	34.55
S1B	44.5	.049	-	-	-	-	-	-
WB, SB, F1B	45.7	.028	-	-	-	-	-	-
W2B, SB, CB	53.8	-	-	-	46.19	50.34	-	-
WB, SB, V1B	-	-	54.8	.040	-	-	-	-
C1B	65.3	.050	65.0	.030	-	-	76.77	72.86
W2T - right wing	83.0	.055	-	-	-	-	-	-
W2T	-	-	87.4	.073	-	-	67.23	70.28
W2T - left wing	87.6	.088	-	-	-	-	-	-
C1B	-	-	-	-	-	-	78.36	-
W2T	-	-	-	-	-	-	83.72	86.62
Wing mode	-	-	-	-	-	-	-	87.88

TABLE III. SCALING RATIOS FOR TFW MODEL.

Scaled quantity	Ratio (model/airplane)
Mach number (M)	1.0
Reduced velocity (V/$\ell\omega$)	1.0
Mass-density (m/$\rho\ell^3$)	1.0
Length (ℓ)	1/5.5
Mass (m)	1/86.43
Density (ρ)	1.925
Velocity (V)	1/2.09
Dynamic pressure (q)	0.4407
Frequency (ω)	2.63
Acceleration	1.258
Force	1/68.64
Bending moment	1/377.53

Matched point from which ratios were derived:

M_{MODEL} = 0.90 in freon

q_{MODEL} = 12.69 kPa (265 lb/ft^2)

V_{MODEL} = 137.7 m/sec (451.8 ft/sec)

$M_{AIRPLANE}$ = 0.90 — standard day air

ALTITUDE = 5,547 m (18,200 ft.)

$V_{AIRPLANE}$ = 287.5 m/sec (943.2 ft/sec)

TABLE IV. TFW MODEL RESPONSE TO UNIT ATMOSPHERIC GUST PSD IN FULL-SCALE UNITS

Response	Mach number	TFW constraint	Experimental $\bar{A}$	Experimental N_0	Calculated GVT modes $\bar{A}$	Calculated GVT modes N_0	Calculated NASTRAN modes $\bar{A}$	Calculated NASTRAN modes N_0
			g	Hz	g	Hz	g	Hz
Pilot-station vertical acceleration	0.65	Free	0.0167	1.89	0.011	1.65	0.016	1.14
		Locked	.0154	1.70	.012	1.24	.013	1.14
	0.90	Free	.0195	2.20	.019	2.14	.023	1.77
		Locked	.0166	1.30	.027	1.37	.023	1.62
Mid-point vertical acceleration	0.65	Free	.0172	2.00	.013	1.54	.018	1.26
		Locked	.0178	1.57	.014	1.29	.016	1.23
	0.90	Free	.0217	2.19	.024	2.05	.028	1.89
		Locked	.0188	1.92	.032	1.52	.029	1.76
Model c.g. vertical acceleration	0.65	Free	.0197	2.11	.014	1.56	.019	1.31
		Locked	.0208	1.68	.015	1.34	.017	1.30
	0.90	Free	.0254	2.26	.027	2.67	.030	1.94
		Locked	.0224	2.05	.035	1.61	.032	1.84
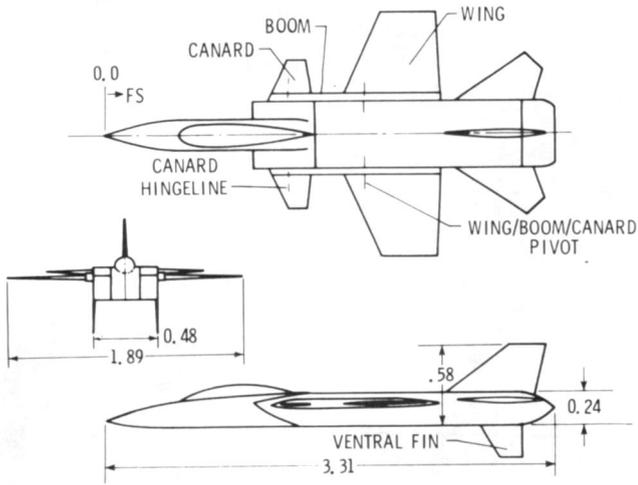
(a) 3-view sketch of complete model.

Figure 1.- Sketches of Torsion-Free-Wing (TFW).
All dimensions are in meters.
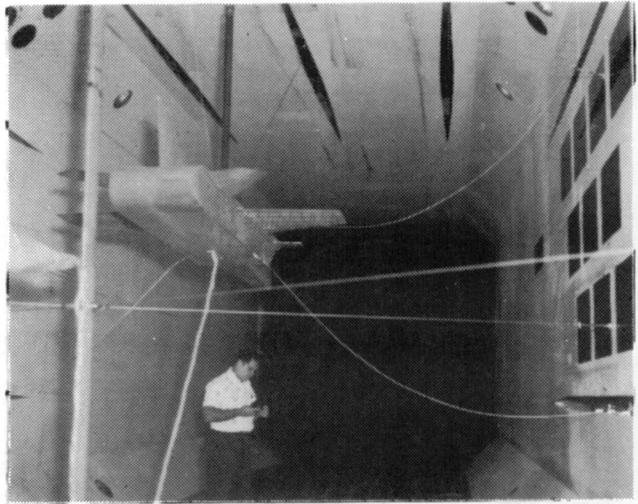
(b) Model mounted on cable-mount system.

Figure 2.- Concluded.
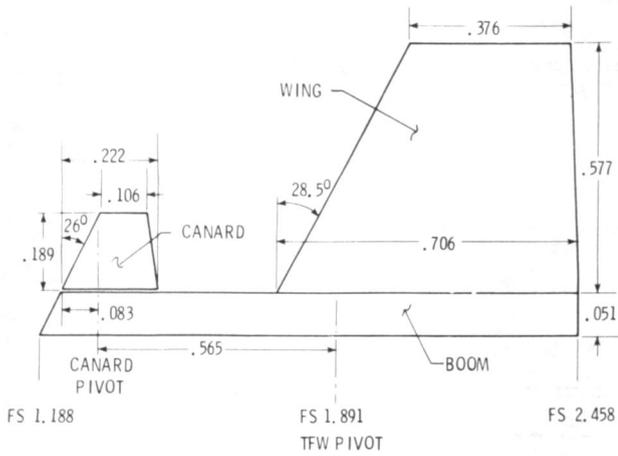
(b) Sketch of TFW semispan.

Figure 1.- Concluded.
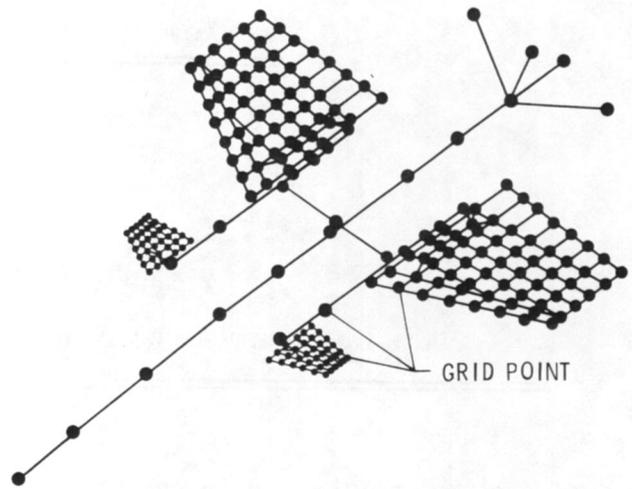
Figure 3.- NASTRAN finite-element representation of
model structure.
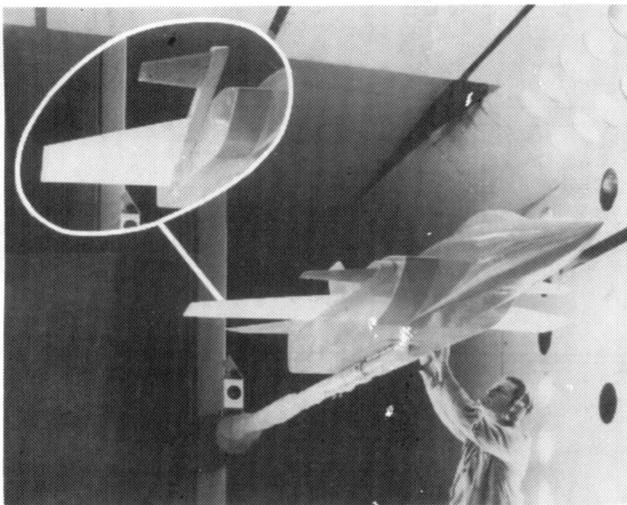
(a) Model mounted on sting.

Figure 2.- Torsion-free-wing model in Langley
Transonic Dynamics Tunnel.

MEASURED (GVT) MODES

WING FIRST BENDING   WING FIRST TORSION

f = 13.7 Hz   f = 36.3 Hz

CALCULATED (NASTRAN) MODES

f = 14.25 Hz   f = 33.2 Hz   f = 34.75 Hz
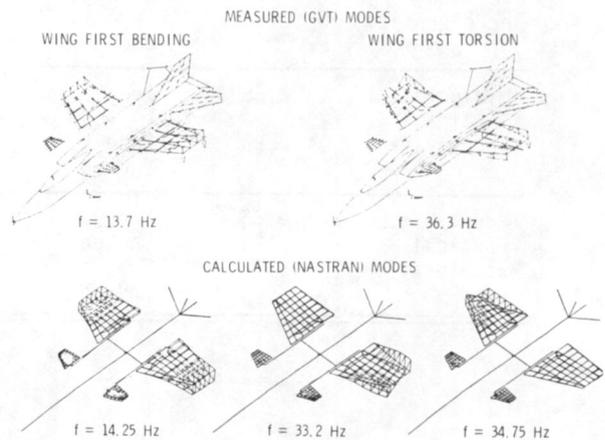
(a) TFW-free configuration.

Figure 4.- Measured and calculated vibration
characteristics of fundamental symmetric
flexible modes of model.

12

MEASURED (GVT) MODES

WING FIRST BENDING   WING FIRST TORSION (LEFT WING)

f = 12.6 Hz   f = 36.0 Hz

CALCULATED (NASTRAN) MODES

f = 12.67 Hz   f = 32.96 Hz   f = 34.55 Hz
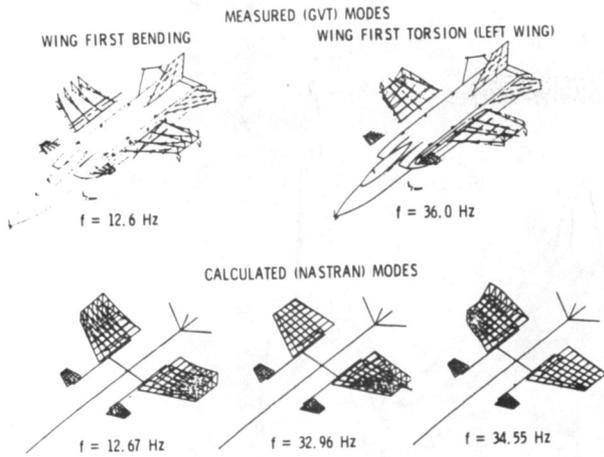
(b) TFW-locked configuration

Figure 4.- Concluded.

Figure 5.- View of airstream oscillator vane system showing cutaway of mechanism.
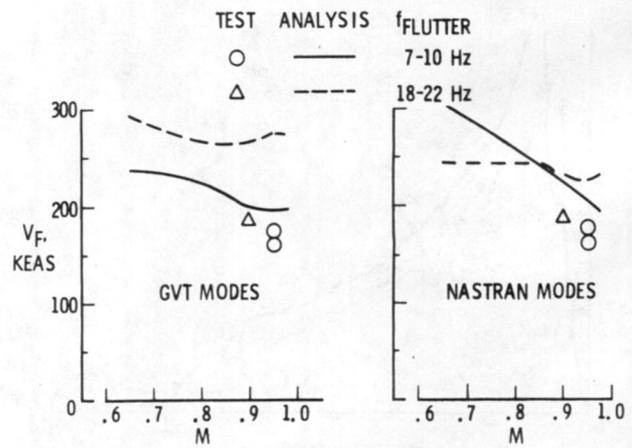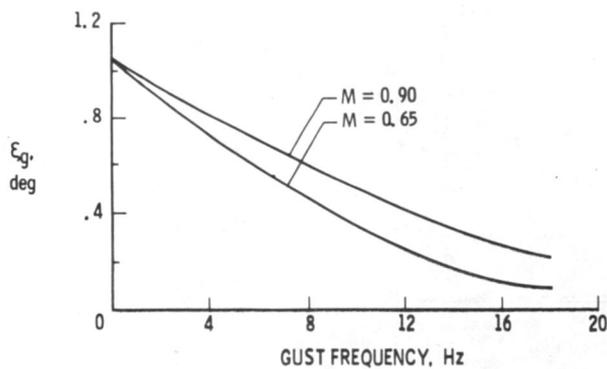
Figure 6.- Variation of wind-tunnel gust amplitude with frequency.

Figure 7.- Experimental flutter boundaries.

(a) TFW-free configuration.
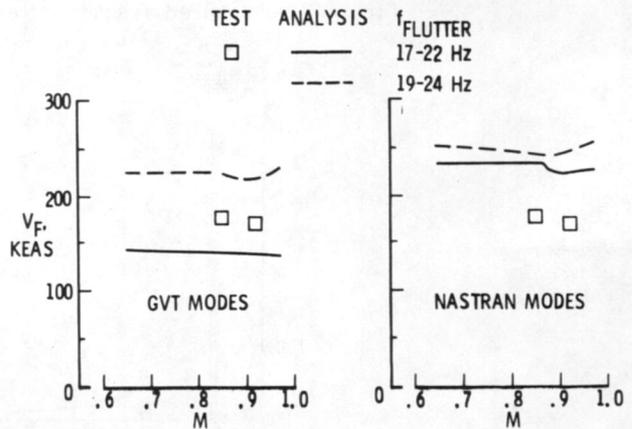
(b) TFW-locked configuration.

Figure 8.- Comparison of experimental and calculated flutter boundaries.
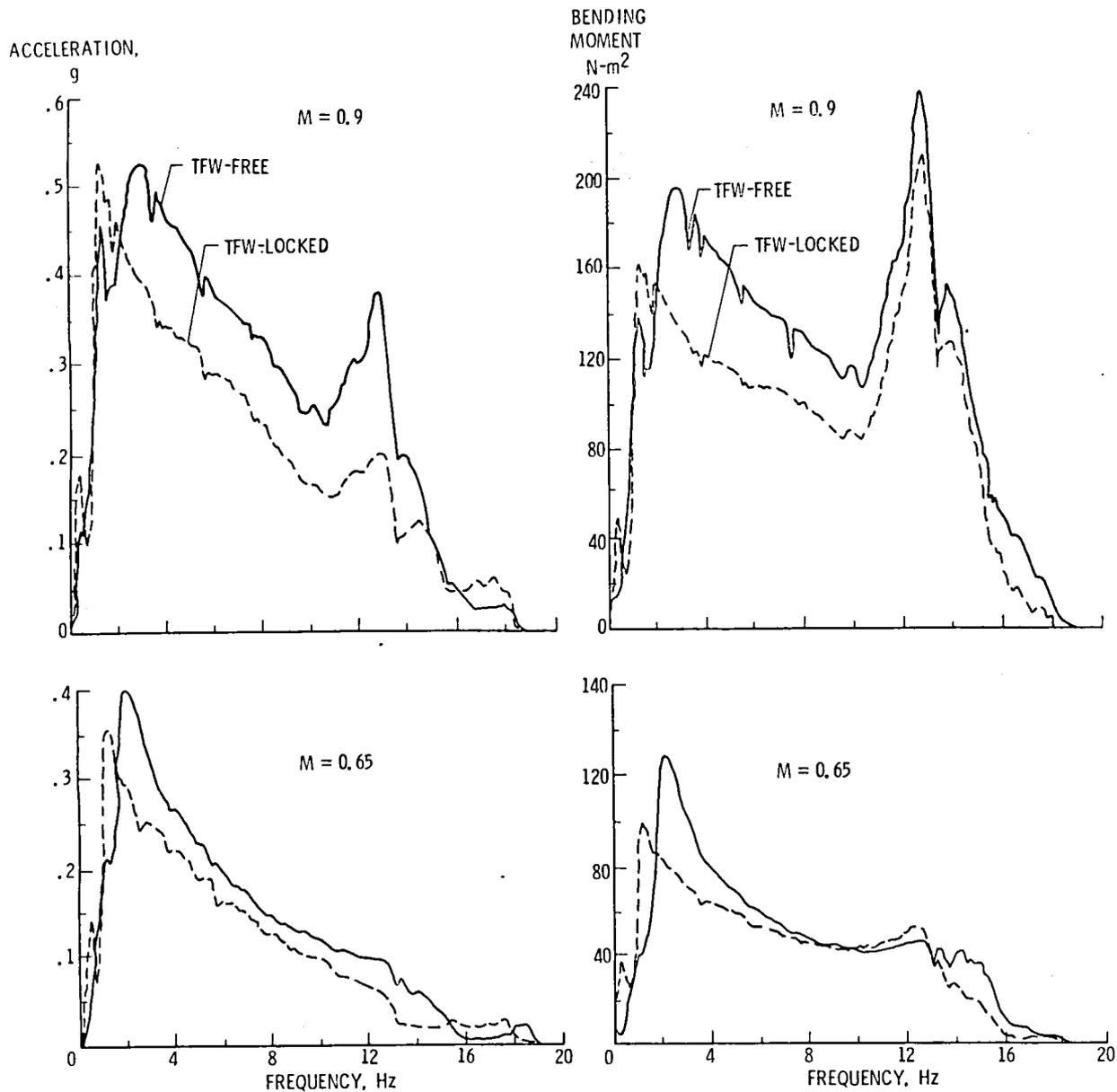
(a) Vertical accelerations at pilot-station.   (b) Bending moments at left-wing root.

Figure 9.- Measured frequency responses to wind-tunnel gusts.
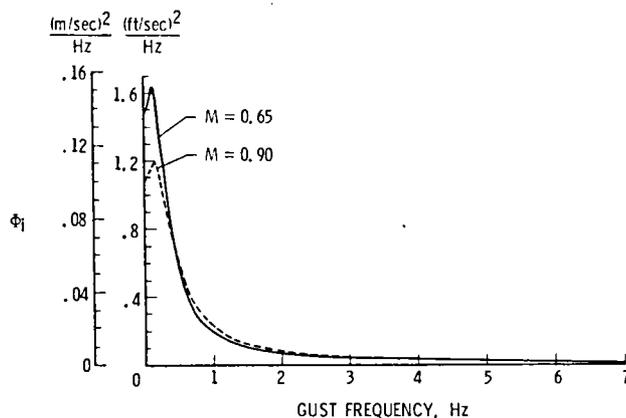
Figure 10.- Von Karman atmospheric gust power-spectral-density function (Φ_i) in full-scale airplane units.
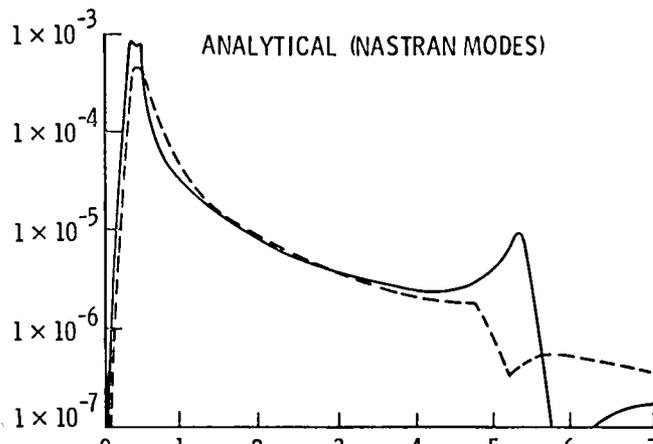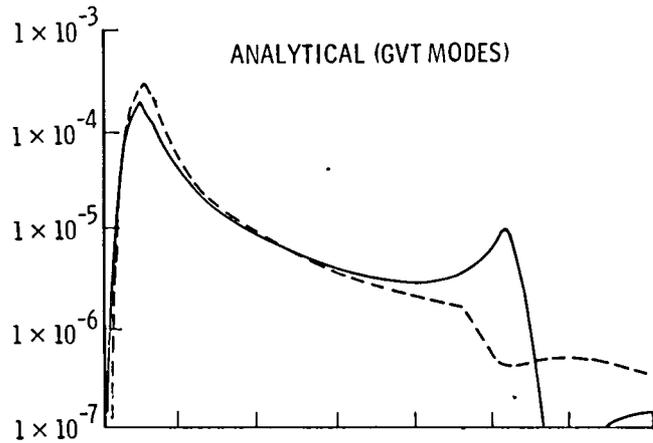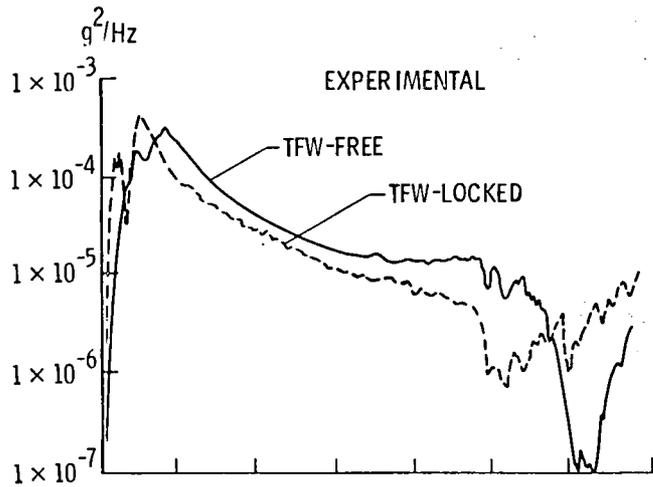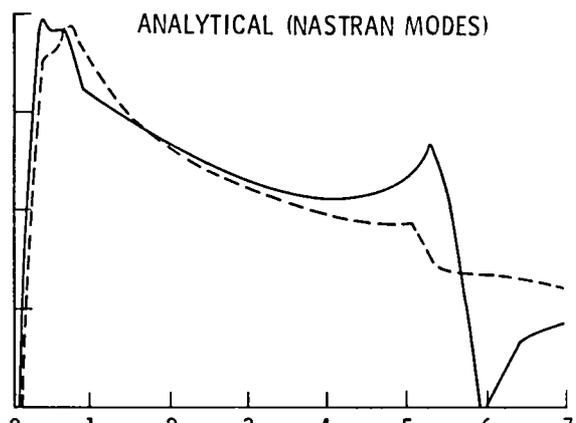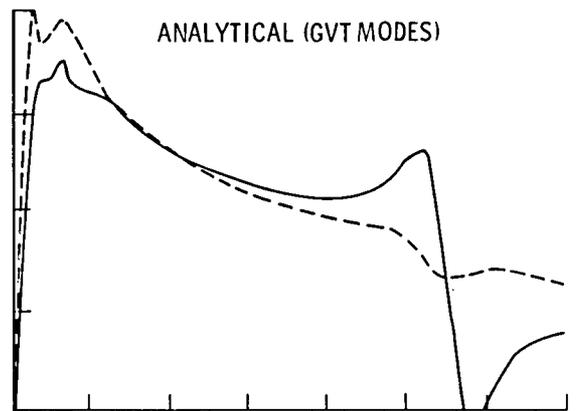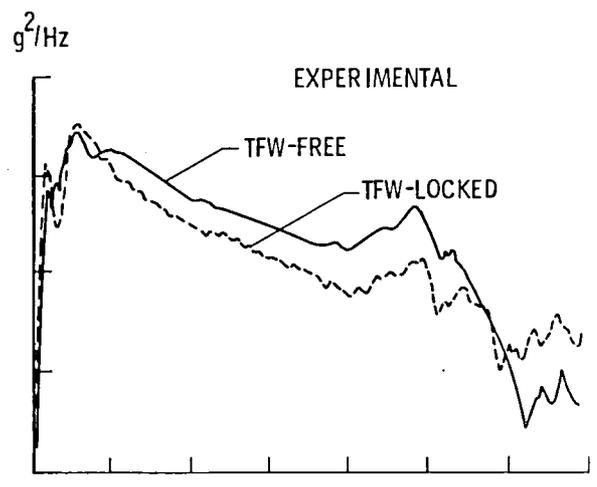
Figure 11.- Experimental and analytical responses to Von Karman atmospheric gust turbulence. Response power-spectral densities (PSD) are for vertical accelerations at pilot-station in full-scale airplane units.

1. Report No. NASA TM -81961	2. Government Accession No.	3. Recipient's Catalog No.
4. Title and Subtitle Transonic Flutter and Gust-Response Tests and Analyses of a Wind-Tunnel Model of a Torsion-Free-Wing Airplane		5. Report Date April 1981
		6. Performing Organization Code 505-33-53-01
7. Author(s) Charles L. Ruhlin and Arthur C. Murphy*		8. Performing Organization Report No.
		10. Work Unit No.
9. Performing Organization Name and Address NASA Langley Research Center Hampton, VA 23665		
		11. Contract or Grant No.
		13. Type of Report and Period Covered Technical Memorandum
12. Sponsoring Agency Name and Address National Aeronautics and Space Administration Washington, DC 20545		
		14. Sponsoring Agency Code

15. Supplementary Notes

16. Abstract

An exploratory study of a 1/5.5-size, complete-airplane version of a torsion-free-wing (TFW) fighter aircraft was conducted in the Langley Transonic Dynamics Tunnel. The TFW consisted of a wing/boom/canard assembly on each fuselage side that was interconnected by a common pivot shaft so that the TFW could rotate freely in pitch. The effect of the TFW was evaluated by comparing data obtained with the TFW free and the TFW locked to the fuselage. With the model mounted on cables to simulate an airplane free-flying condition, flutter boundaries were measured at Mach numbers (M) from 0.85 to 1.0, and gust responses at $M = 0.65$ and 0.90. The critical flutter mode for the TFW-free configuration was found experimentally to occur at $M = 0.95$ and had the rigid-TFW pitch mode as its apparent aerodynamic driver. However, the minimum flutter dynamic pressure for the TFW-free case was only about 20 percent lower than for the TFW-locked; therefore, the present TFW is considered to be a viable design concept, with respect to flutter. The present TFW was not effective as a gust alleviator. Analyses of the vibration, flutter, and gust-response characteristics were made using a finite-element representation and aerodynamic terms based on lifting-surface theory that included interference effects. Although the analyses predicted the flutter-critical modes, the experimental flutter-speed levels and M trends were predicted poorly. The analytical gust-response data correlated reasonably well with the experimental data.

17. Key Words (Suggested by Author(s)) Flutter Gust-Response Torsion-Free-Wing Airplane Wind-Tunnel Test	18. Distribution Statement Unclassified - Unlimited Subject Category - 05
19. Security Classif. (of this report) Unclassified	20. Security Classif. (of this page) Unclassified	21. No. of Pages 15	22. Price* A02